ACS APPLIED MATERIALS & INTERFACES

Research Article

www.acsami.org

Electrochemical Preparation and Characterization of Polypyrrole/Stainless Steel Electrodes Decorated with Gold Nanoparticles

Eduart Gutiérrez Pineda,[†,‡] Francisco Alcaide,[¶] María J. Rodríguez Presa,[†] Agustín E. Bolzán,*[,†] and Claudio A. Gervasi*[,†,‡]

[†]Instituto de Investigaciones Fisicoquímicas Teóricas y Aplicadas (INIFTA), Universidad Nacional de La Plata - CONICET, Sucursal 4 Casilla de Correo 16, 1900 La Plata, Argentina

[‡]Laboratorio de Investigaciones de Metalurgia Física (LIMF), Facultad de Ingeniería, Universidad Nacional de La Plata, 1900 La Plata, Argentina

[¶]CIDETEC, Parque Científico y Tecnológico de Guipúzcoa, Paseo Miramón, 196 20009, Donostia-San Sebastián, Guipúzcoa, Spain

ABSTRACT: The electrosynthesis and characterization of polypyrrole(PPy)/stainless steel electrodes decorated with gold nanoparticles and the performance of the composite electrode for sensing applications is described. PPy films were grown in potassium perchlorate and sodium salicylate solutions under comparable electropolymerization conditions. Polymer films prepared in the presence of perchlorate ions exhibited worm-like structures, whereas columnar structures were obtained in salicylate-containing solutions. Voltammetric response of PPy films prepared in salicylate solutions was more reversible. PPy films were decorated with gold nanoparticles obtained by a double step potentiostatic electrodeposition routine that allowed fine control of deposit characteristics. Analysis of deposits was performed by means of SEM and confocal Raman spectroscopy. The electrocatalytic activity of the Au/PPy electrodes was assessed for the electro-oxidation of hydrazine and hydroxylamine. Results showed a successful optimization of the route of synthesis that rendered nanocomposite electrode materials with promising applications in electrochemical sensing.

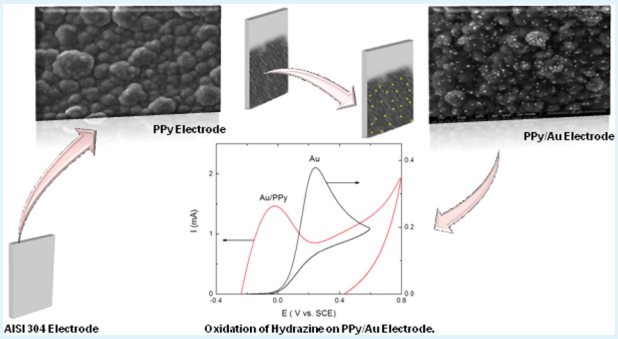

KEYWORDS: *gold nanoparticles, polypyrrole, stainless steel, electrodeposition, hydrazine, hydroxylamine, sensors*

1. INTRODUCTION

Polypyrrole (PPy) is a polymer that exhibits reasonably high conductivity and good chemical stability and can be prepared in aqueous solutions.[1] These characteristics have promoted PPy as one of the most versatile conductive polymers in electrochemistry, with widespread use in sensors,[2,3] corrosion protection,[4−6] batteries,[7,8] and supercapacitors.[9,10] PPy films are conductive in the oxidized state and their physical and spectroscopic properties depend strongly on the preparation method, i.e., nature of the solvent, supporting electrolyte, solution pH, monomer concentration, and electrodeposition routine. This means that, for instance, by changing the supporting electrolyte the film morphology can be modified from a compact to a porous, open one. Thus, spherical particles were produced using potassium tetraoxalate,[11] large porous structures using dodecyl sulfate,[2] nanowires using lithium perchlorate,[12] or hollow microtubes of rectangular cross-section using salicylate solutions.[13]

PPy films are suitable matrices for the fabrication of composite electrodes when combined with metal nanoparticles. Particularly, for gold nanoparticles (GNPs), the porous structure of the PPy film can provide low ohmic-drop pathways while the deposition of a suitable array of the GNPs could increase the rate constant of an electron transfer process taking place on the metallic surface. GNPs are of particular interest due to the outstanding electrocatalytic and optical properties that, in addition to good biocompatibility, make them an attractive material for designing electrochemical sensors and biosensors.[14] The increasing awareness of developing electrochemical sensors based on GNPs deposited on polymeric films resides in the fact that, contrary to flat smooth gold electrodes used for sensing, Au/PPy nano and microstructures provide large active surface area films whose thickness and morphology can be varied according to the experimental production conditions. Furthermore, simultaneous formation of a GNPs deposit and conducting polymer film resulted in good sensitivity, catalytic properties, and conductivity of the composite material.[15] Most of the desirable properties of metallic nanoparticle-containing composites depend on the possibility of producing an array of well-distributed metallic nanoparticles on the surface of the conducting support. For instance, GNPs have been embedded in three-dimensional sol−

Received: November 5, 2014
Accepted: January 8, 2015
Published: January 8, 2015

DOI: 10.1021/am507733b
ACS Appl. Mater. Interfaces 2015, 7, 2677−2687

gel networks,[16] electrodeposited on choline films formed on glassy carbon electrodes,[17] electrodeposited on ultrathin overoxidized PPy films on glassy carbon,[2] codeposited under galvanostatic conditions to form a nanocomposite with PPy on GC,[18] and deposited on PPy nanowires[12] or graphite pencil electrodes,[19] among other examples. Deposition of gold particles has been carried out under galvanostatic,[18,20,21] potentiostatic,[11] and potential cycling[12,14,17,22] conditions or by simple immersion of electrodes in a gold ion-containing solution.[19,23]

In this work we report on the preparation and characterization of composite electrodes obtained by electrodeposition of GNPs on PPy films that were previously synthesized by electropolymerization from electrolytes containing different types of counterions. Stainless steel (SS) substrates were of different forms (plate and mesh) and final electrode characteristics were optimized to be used for hydrazine and hydroxylamine detection. The use of SS as substrate for PPy films opens up the possibility of employing a comparatively low-cost stable material easily shaped in different forms like rods, plates, meshes, etc. The PPy film on a SS substrate not only provides the support for the deposition of GNPs, but also acts as corrosion inhibitor.[4,24] Protection of SS substrates by deposition of polymer films is a well-known technique.[5,6,25−27]

Decoration of the PPy matrix with GNPs through electrodeposition at constant potential allows gain of a fine control of the amount and size of the particles. Surface morphology, as well as structural, optical, and electrochemical properties of the composite electrode, were characterized by using scanning electron microscopy (SEM), atomic force microscopy (AFM), energy dispersion spectroscopy (EDX), Raman spectroscopy, cyclic voltammetry, and electrochemical impedance spectroscopy (EIS). Potential application of the resulting composite electrodes to the development of electrochemical sensors was demonstrated by studying the voltammetric electro-oxidation of hydroxylamine and hydrazine, two molecules whose detection and quantitative determination in aqueous solutions are relevant to the chemical, pharmaceutical, agricultural, and food industries.[28]

2. EXPERIMENTAL METHODS

2.1. Reagents. Distillation under reduced pressure was used to purify Pyrrole (Sigma-Aldrich) which was maintained in a refrigerator under nitrogen atmosphere in darkness before use. For Au electrodeposition $HCl_4Au{\cdot}3\ H_2O$ (Aldrich, p.a.) was used, and for the electrochemical oxidation of hydrazine and hydroxylamine, $N_2H_5HSO_4$ (Fluka, p.a.) and NH_2OH (Fluka, p.a.) were employed, respectively. All solutions were prepared with Milli-Q water. After deposition, the PPy films were washed with Milli-Q water or ethanol (96% v/v Sigma-Aldrich).

2.2. Electrode Preparation. SS substrates were made of grade AISI 304 (UNS S30400) with weight percentage composition as follows: 0.070% C, 1.61% Mn, 0.43% Si, 0.022% P, 0.005% S, 8.33% Ni, 17.94% Cr, 0.03% V, 0.04% Nb, 0.34% Mo, 0.22% Co, 0.20% Cu, and 0.001% Ti and Fe balance. SS plates (0.45 cm^2) were mechanically grounded with emery paper (grit 1000) and afterward immersed in 1:1 v/v H_2SO_4/HNO_3 solution for 15 s, washed, and sonicated for 15 min in Milli-Q water to obtain a clean starting surface. SS wire meshes (made from wire of 100 μm in diameter and a width of mesh of 200 μm) were cut into samples of dimensions (0.5 × 0.5) cm^2. Mesh substrates were cleaned chemically before the experiments by immersion in 1:1 v/v H_2SO_4/HNO_3 solution for 15 s, and subsequently washed and sonicated for 15 min in Milli-Q water. A conventional three-electrode cell was used for the formation of the PPy layer on the SS substrate. The electropolymerization of PPy was carried out at constant potential (E = 0.80 V) during either 5 or 10 min in aqueous 0.25 M pyrrole + 0.1 M $KClO_4$ or 0.25 M pyrrole + 0.5 M $C_7H_5NaO_3$.

Au electrodeposition on the PPy/SS electrodes was performed in 0.001 M $HAuCl_4$ + 0.005 M H_2SO_4 solution using a double step potentiostatic routine. Initially the working electrode potential was set to 0.8 V during 10 s to activate/clean the electrode. Afterward, the potential was stepped to −0.8 V during 0.1−0.5 s, to allow the formation of Au nuclei on the PPy surface, and eventually stepped to 0.1 V during 0.5−60 s to grow the Au nuclei previously formed.

2.3. Instruments and Experimental Techniques. Voltammetry and chronoamperometry measurements were made using a Voltalab 10 (Radiometer Analytical) potentiostat. Electrochemical impedance spectroscopy measurements were carried out by using a Zahner IM6d electrochemical workstation. For EIS experiments the amplitude of the AC signal was 0.01 V and the measuring frequency f was varied in the $10^{-3} \leq f \leq 60 \times 10^3$ Hz range. Electrochemical experiments were made at room temperature under nitrogen atmosphere. Potentials are referred to the saturated calomel electrode (SCE) scale.

The morphological characterization of PPy and Au/PPy deposits was made by using an environmental scanning electron microscope (FEI Quanta 200 ESEM, accelerating voltage 12−15 kV, Everhardt-Thornley detector) equipped with and Oxford Inca 300 EDX system for chemical analysis. Surfaces of the samples were also examined with an atomic force microscope (Veeco Multimode AFM) connected to a Nanoscope V controller.

Raman and confocal Raman spectra were obtained using a Renishaw 2000 spectrometer with a He−Ne laser (wavelength 633 nm). Renishaw in Via microscope collects Raman spectra at standard or high confocality mode, giving high spatial resolution (<1 μm lateral). Raman microscope is fitted with two lasers 532 and 785 nm, CCD camera, internal calibration source, motorized stage controlled by Wire 2.0 software.

Qualitative evaluation of changes in adherence of PPy films to the substrate was performed according to the standard sellotape test (ASTM test method D 3359).

3. RESULTS AND DISCUSSION

Black PPy films electroformed at a potential of 0.8 V during either 5 or 10 min of electrolysis in both $KClO_4$ and $C_7H_5NaO_3$ solutions exhibit properties that depend on both the supporting electrolyte and the type of substrate employed. Thus, for a fixed growth time, thicker and less adherent films were obtained in $KClO_4$ solutions. Anodic charge for the potentiostatic growth of PPy films varied from ca. 1.85 C cm^{-2} to 6.50 C cm^{-2} in $KClO_4$ solutions and from ca. 0.5 C cm^{-2} to 1.6 C cm^{-2} in $C_7H_5NaO_3$ solutions, when the growth time increased from 5 to 10 min. Based on the classification chart of ASTM sellotape test, adherence was estimated to be class 4B and 2B for PPy films formed in salicylate and perchlorate solutions, respectively. However, these results should be taken with caution due to the nonuniform nature of the film thickness. Nevertheless, high adherence values that characterize resistance to the mechanical stress applied in the sellotape test are less relevant in our case than in the case of PPy films used as coatings for corrosion protection.

3.1. Electrochemical Characterization of PPy-Modified SS. The electrochemical behavior of PPy films formed at 0.8 V during either 5 or 10 min on SS substrates in mesh or plate forms was characterized by both voltammetric scans and impedance spectroscopy measurements. Cyclic voltammograms of the PPy/SS electrode run between −0.8 and 0.6 at 0.005 V s^{-1} are strongly dependent on the electrolyte composition. Thus, in $KClO_4$ solution, the voltammogram exhibits an anodic current peak at ca. 0.2 V and a cathodic current peak at ca. −0.37 V. Additionally, a large current envelope due to the

DOI: 10.1021/am507733b
ACS Appl. Mater. Interfaces 2015, 7, 2677−2687

capacitive contribution of PPy film is clearly present in the whole potential window scanned in each voltammetric cycle (Figure 1). However, after immersing the PPy/SS electrode in

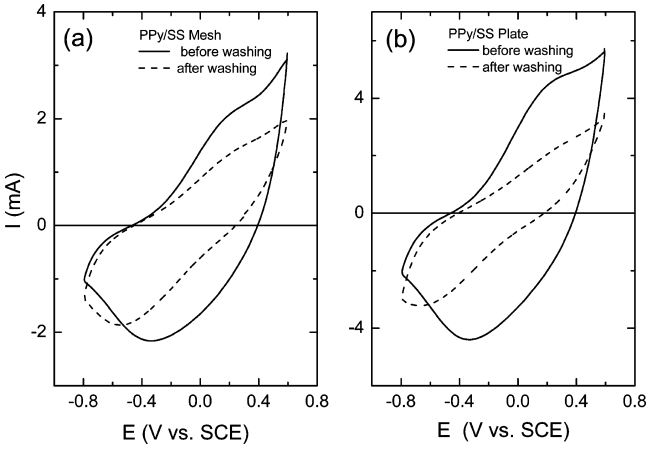

Figure 1. Cyclic voltammograms run at 0.005 V s^{-1} for PPy/SS electrodes in 0.1 M $KClO_4$ before and after immersion in water. PPy films produced at 0.8 V in 0.25 M Py + 0.1 M $KClO_4$ during 5 min.

Milli-Q water for 10 min, a significant decrease in both the anodic and cathodic charge and the reversibility of the electrochemical processes are clearly observed: current peaks appear poorly defined and superimposed on a sloping resistive line.

In salicylate electrolyte (Figure 2) more reversible voltammetric peaks are observed that appear at more negative

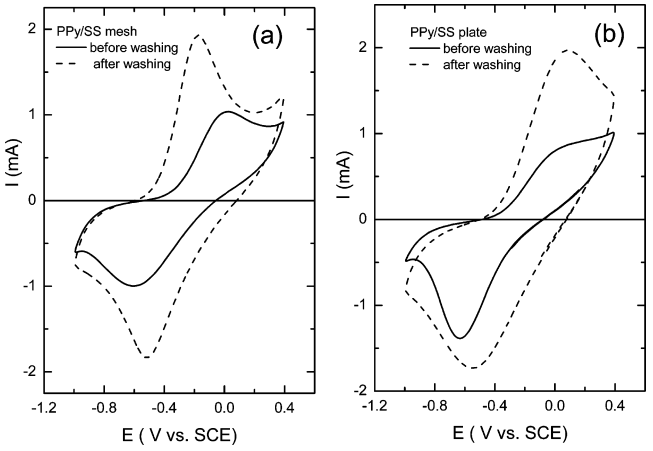

Figure 2. Cyclic voltammograms run at 0.005 V s^{-1} of PPy/SS electrodes in 0.5 M $C_7H_5NaO_3$ before and after immersion in ethanol. PPy films produced at 0.8 V in 0.25 M Py + 0.5 M $C_7H_5NaO_3$ during 5 min.

potentials, namely, −0.2 and −0.5 V, respectively. After immersing the electrode in ethanol, well-defined peaks with larger redox currents are recorded, a fact that may be due to dissolution of a fraction of deposited monosodium salicylate species trapped inside the polymer during film growth, but not participating in the charge balance process associated with the film oxidation. This, in turn, could lead to a larger polymer surface exposed to the solution and to a decrease in the ohmic resistance contribution due to the salt deposit. The change in the position of the current peaks could be associated with the low diffusivity of large-size salicylate anions or their immobilization inside the polymer matrix determining charge compensation by cations and, consequently, polymer conformational changes. Such conformational changes are believed to be responsible for the shift of the anodic and cathodic peak potentials toward more negative values.[29] On the other hand, the integrated charges under the oxidation and reduction peaks are very similar. Thus, the Coulombic efficiency over a cycle of charge/discharge is approximately 100%.

EIS is a powerful and firmly established technique for examining the properties of surface-modified electrodes. It has been widely used for the qualitative and quantitative characterization of electrochemical processes occurring in conductive polymer films.[20−22,30] Therefore, to characterize the PPy/SS electrodes, EIS measurements were made at the open circuit potential (OCP) and at different potentials in the potential window OCP ± 0.20 V for both types of SS substrates and electrolytes. The OCP in 0.1 M $KClO_4$ was about 0.27 V, shifting to less positive potentials after immersion in water (ca. 0.12 V), whereas for $C_7H_5NaO_3$ solutions, the OCP was found to be about −0.12 V before and −0.06 V after immersion in ethanol, respectively.

The "ideal" impedance response of an electrode modified with an electroactive polymer film is well established and corresponds to separate Randles circuit behavior at high frequencies, a Warburg section at intermediate frequencies, and a purely capacitive behavior due to the redox capacitance at low frequencies. In our experiments typical deviations are encountered. Nonuniform film thickness is one of the effects that can be taken into account to explain the differences between ideal and real responses. When the film consists of thin and thick regions, no Warburg section appears. Moreover, complex impedance plots with finite slopes in the low-frequency region are obtained by considering a distribution of thickness values. Thus, Nyquist plots obtained for the PPy films in $KClO_4$ solution display a single time constant at frequencies above 0.6 Hz due to the charge transfer or redox process of the PPy matrix. This loop is followed by an almost purely capacitive response at low frequencies, particularly at the OCP (Figure 3). In agreement with the voltammetric data the charge transfer resistance increases after immersing the electrode in Milli-Q water (Figure 3). Furthermore, as the electrode potential is shifted away from the OCP, the charge transfer resistance increases, particularly at potentials more negative than the OCP, as expected for a polymer film that decreases its conductivity in the reduced state.[31] The effect of a distribution in polymer layer thickness L on the impedance response recorded at low frequency is to decrease the tilt angle of the linear behavior respect to a vertical line. The tilt angle decreases as the value of the spread factor increases. The spread factor measures how inhomogeneous the film is due to variations in morphology from one region to another.[32]

On the other hand, the Nyquist plots recorded in $C_7H_5NaO_3$ solution for PPy films obtained in the same solution also show a single time constant at high frequencies while the capacitance response at low frequencies is no longer observable (Figure 4a). Thus, the whole dynamic behavior in the studied frequency range is dominated by the redox process alone. A decrease in the charge transfer resistance was recorded after immersing the electrode in ethanol for 10 min (Figure 4b), something that agrees with the voltammetric response and again represents the opposite behavior to PPy-modified electrodes in $KClO_4$ solutions.

DOI: 10.1021/am507733b
ACS Appl. Mater. Interfaces 2015, 7, 2677−2687

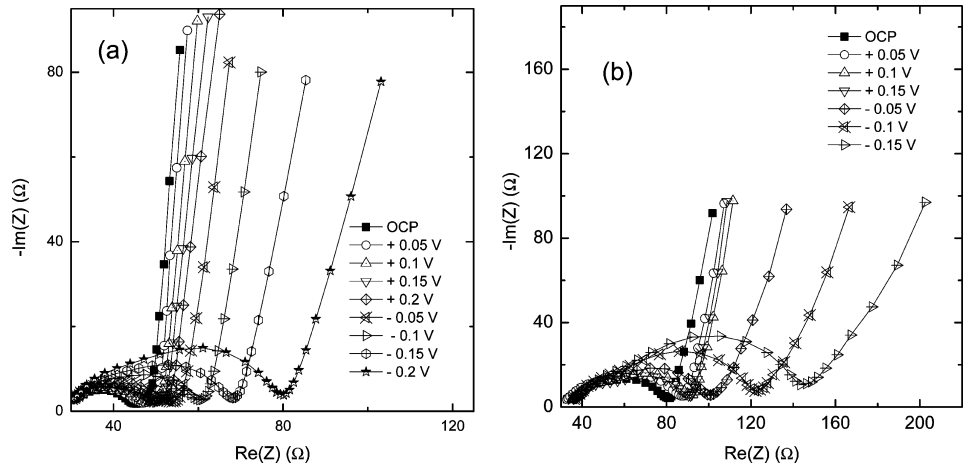

Figure 3. Nyquist plots recorded at different potentials for a PPy/SS electrode in 0.1 M $KClO_4$ before (a) and after (b) immersion in water during 10 min. PPy film was formed in 0.1 M $KClO_4$ at 0.8 V during 5 min.

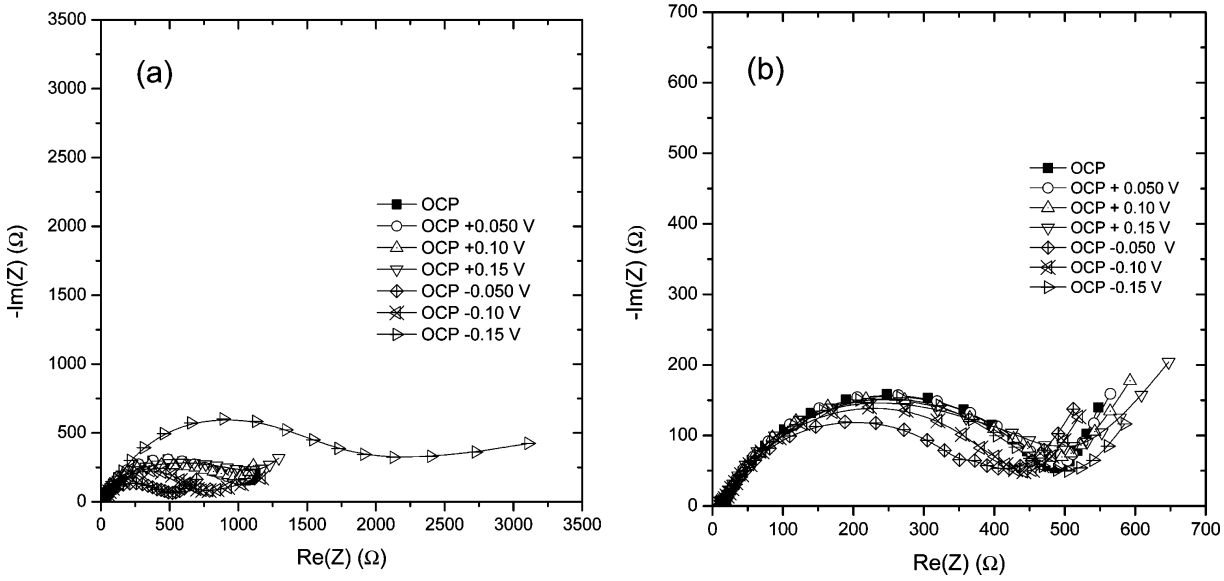

Figure 4. Nyquist plots recorded at different potentials for a PPy/SS electrode in 0.5 M $C_7H_5NaO_3$ before (a) and after (b) immersion in ethanol during 10 min. PPy film was formed in 0.5 M $C_7H_5NaO_3$ at 0.8 V during 5 min.

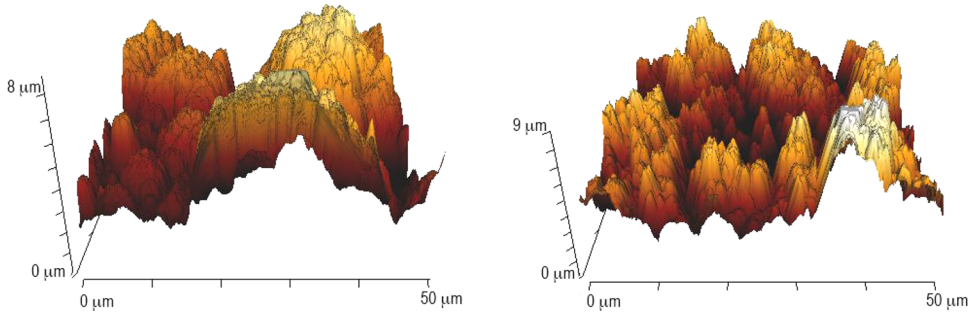

Figure 5. 3D AFM images corresponding to a PPy film formed on a SS plate electrode at 0.8 V during 10 min in 0.1 M $KClO_4$ (left) and 0.5 M $C_7H_5NaO_3$ (right).

3.2. AFM Imaging of PPy films on SS Electrodes. AFM images obtained from PPy films grown on SS plates show the presence of rounded domains in the case of films produced in $KClO_4$ solutions, and rather columnar spiked formations when the films were grown in $C_7H_5NaO_3$ solutions (Figure 5). The latter is in agreement with AFM data reported for PPy films grown in $C_7H_5NaO_3$ solutions, which showed the formation of PPy microtubes in the films, after immersion in ethanol.[13] Cross-section profiles of the PPy films shows that both the *rms* and the average roughness of the film increases when the electrolyte is changed from $KClO_4$ to $C_7H_5NaO_3$. Thus, in the former case, due to the formation of relatively larger globular

DOI: 10.1021/am507733b
ACS Appl. Mater. Interfaces 2015, 7, 2677−2687

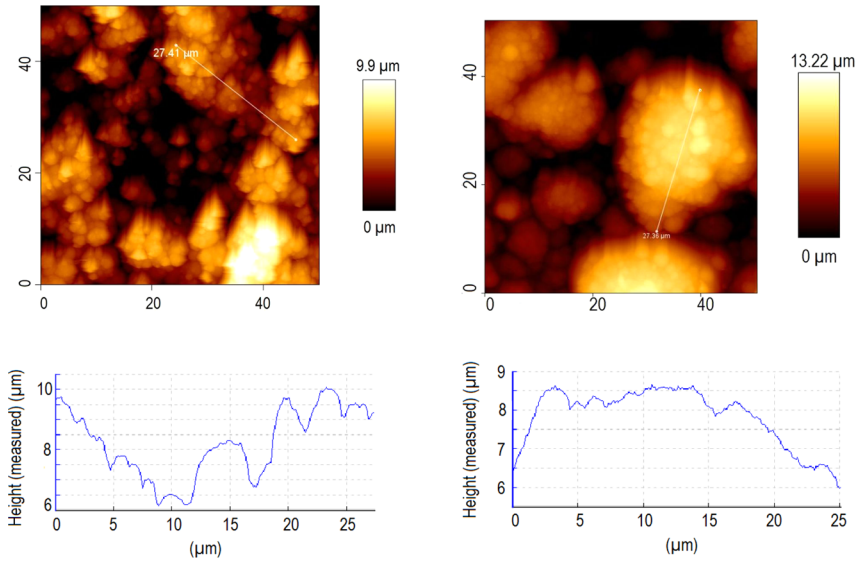

Figure 6. Topography with cross-section lines (above) and profiles (below) of AFM images corresponding to PPy films grown during 10 min in 0.5 M $C_7H_5NaO_3$ (left, *rms* = 1.42 μm and average roughness 1.21 μm) and 0.1 M $KClO_4$ (right, *rms* = 783 μm, average roughness 648.3 nm).

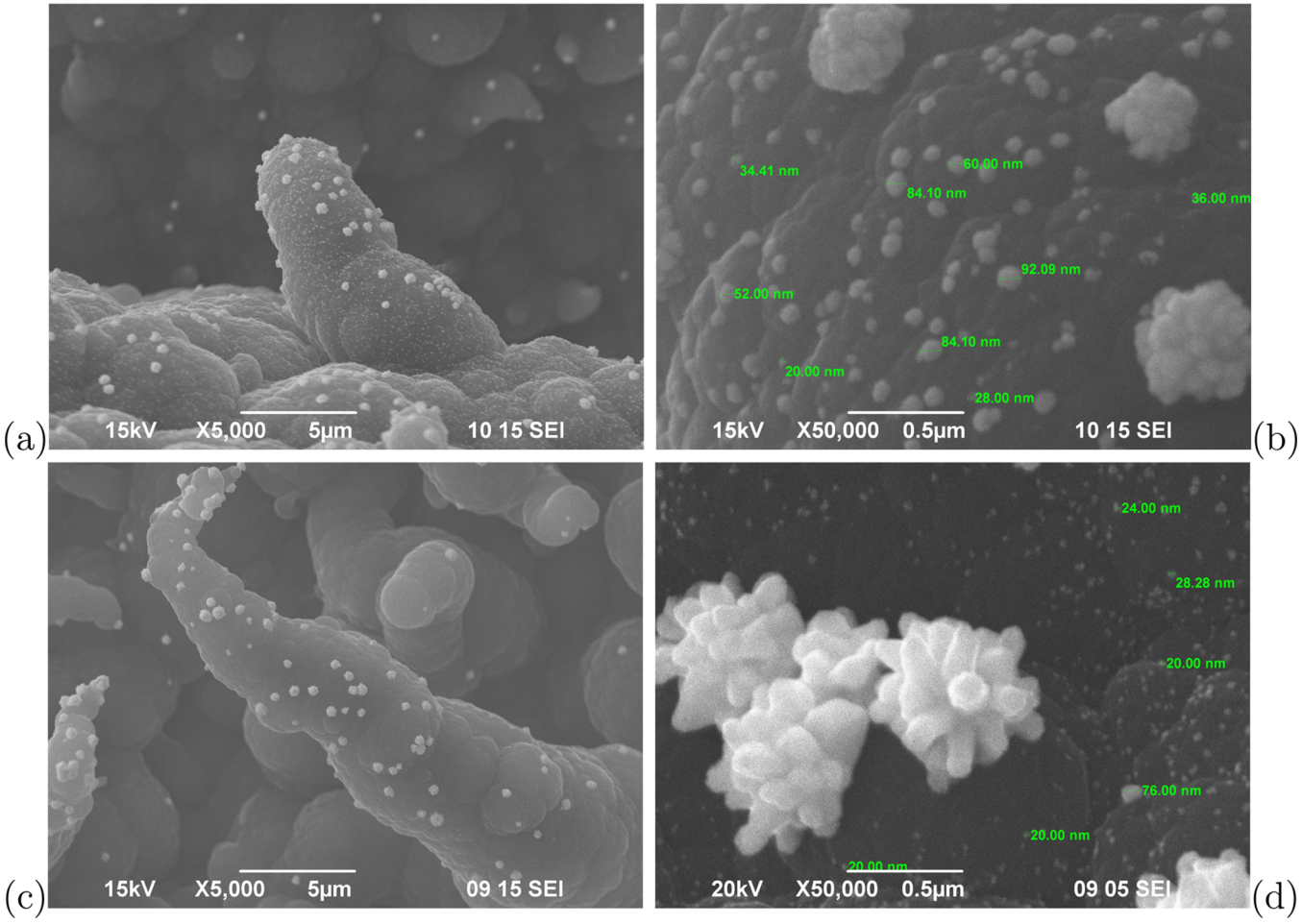

Figure 7. SEM images of gold deposited on PPy films formed on SS mesh (a,b) and plate (c,d). PPy film was formed at 0.8 V during 10 min in 0.1 M $KClO_4$. t_n = 0.5 s, t_g = 10 s (a,b); t_g = 30 s (c), t_g = 60 s (d).

domains, an *rms* of 783 nm is observed, while in the latter, which presents a rather columnar structure, the *rms* increases to 1.42 μm (Figure 6).

3.3. SEM Images and EDX Data of GNPs/PPy Films.

PPy films produced on both plate and mesh SS electrodes in the different electrolytes were decorated with electrodeposited GNPs by applying a double potential step experiment. The

DOI: 10.1021/am507733b
ACS Appl. Mater. Interfaces 2015, 7, 2677−2687

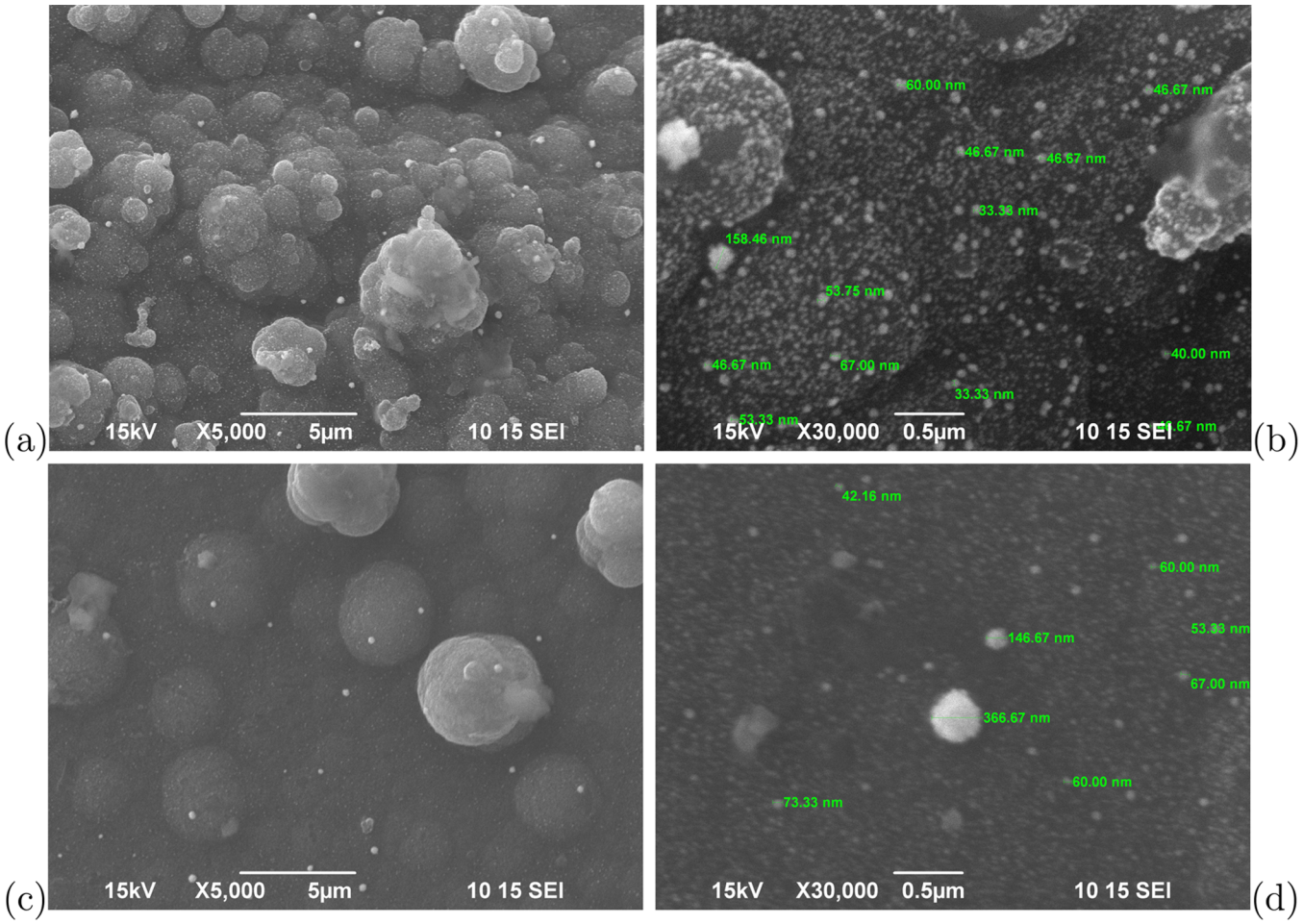

Figure 8. SEM images of gold deposited on PPy films formed on SS mesh (a,b) and plate (c,d). PPy film was formed at 0.8 V during 10 min in 0.5 M $C_7H_5NaO_3$. t_n = 0.5 s (a–d); t_g = 10 s (a,b); t_g = 30 s (c,d).

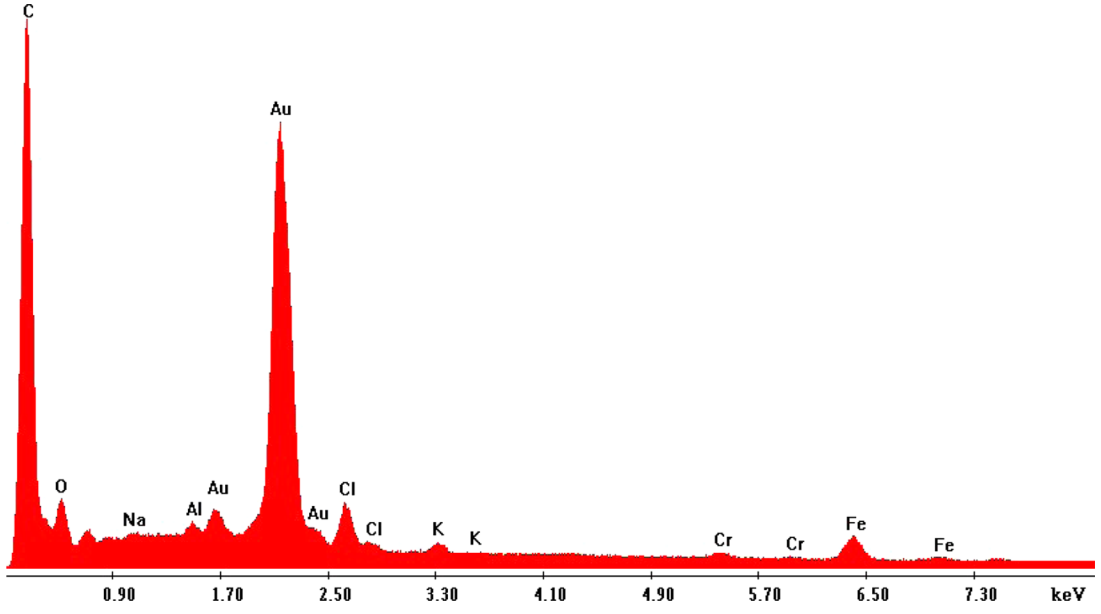

Figure 9. Typical EDX spectra corresponding to PPy/SS electrodes with a gold deposit formed at t_n = 0.1 s, t_g = 1 s. PPy film formed at 0.8 V during 5 min in 0.1 M $KClO_4$.

experiment consisted of a large initial cathodic step at a potential (E = −0.8 V) where the formation of gold nuclei took place for a variable short time (t_n = 0.1–0.5 s) and a subsequent potential step (E = 0.1 V) corresponding to a small cathodic overpotential that was applied for a larger variable time ($5 \leq t_g \leq 180$ s). During t_n an array of well-dispersed GNPs nucleates

DOI: 10.1021/am507733b
ACS Appl. Mater. Interfaces 2015, 7, 2677–2687

while during t_g these GNPs are allowed to grow. Thus, as t_g increases, the particles' size and the deposited Au load increases. This double-step potential routine allows fine-tuned regulation of the electrodeposit characteristics. Moreover, the experimental approach yields a narrow particle-size distribution. For instance, gold electrodeposits obtained for t_n = 0.5 s and t_g = 10 s exhibit in the SEM images the formation of a quite homogeneous distribution of particles in the size range of 20−100 nm. GNPs are accompanied by larger particles disseminated at random on PPy worm-like formations produced in $KClO_4$ solutions (Figure 7) and also on PPy columnar structures produced in $C_7H_5NaO_3$ solutions (Figure 8). To confirm that both the micro- and nanostructured particles corresponded to gold, EDX analysis was routinely performed on the deposits as shown in Figure 9.

A typical voltammogram corresponding to GNP-decorated PPy/SS electrode is shown in Figure 10. It can be observed that the presence of the GNPs on the PPy surface decreases the current contributions due to the reversible processes of the polymer film.

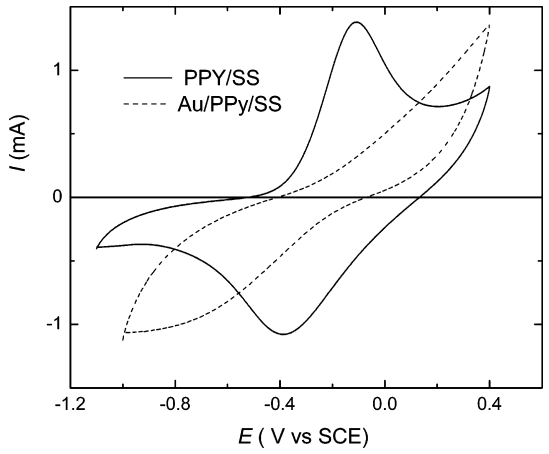

Figure 10. Voltammetric response of GNP-decorated PPy/SS electrode in 0.5 M $C_7H_5NaO_3$. GNPs deposit formed at t_n = 0.1 s, t_g = 30 s. PPy film formed at 0.8 V during 5 min in 0.5 M $C_7H_5NaO_3$. For the sake of comparison, the voltammogram for the PPy-modified electrode prior to the Au electrodeposition is also shown.

3.4. Raman Spectra of PPy/SS and Au/PPy/SS Films. Raman spectroscopy is a standard method for evaluating structural details of PPy.[31] In this work it was used for two purposes, namely, to characterize the films produced in the different solutions and to detect the enhancement of the Raman spectra by the presence of gold particles dispersed on the surface of the PPy film. The latter, as shown below, was particularly useful to estimate the depth inside the polymer film accessible to Au species during deposition. Figure 11 shows the Raman spectra corresponding to Au-free and Au-decorated PPy films obtained in $KClO_4$ and $C_7H_5NaO_3$ solutions. The PPy spectra obtained before the gold electrodeposition show the characteristic bands at ca. 1580−1600 cm^{-1}, which are related to the C═C backbone stretching of PPy[31,33] and those at 1000−1150 cm^{-1}, which have been assigned to the C−H in-plane deformation of oxidized PPy.[34] Once Au has been deposited on the PPy film, the relative intensity of the peaks of Au/PPy film becomes much larger than for pure PPy film. This is due to the SERS effect resulting from the localized surface plasmon resonance that is typical for silver and gold nanoparticles in the 10−200 nm size range.[35] Furthermore, the resulting nanoscale roughness in the Au/PPy film structure is likely to facilitate the charge transfer between pyrrole nitrogen and embedded GNPs.[36] The Raman peak in the range of 1520−1620 cm^{-1} representing the C═C backbone stretching of PPy is related to the conductivity of PPy,[37] i.e., as its wavenumber decreases, the conductivity increases. In the case of PPy films produced in $C_7H_5NaO_3$ solution, it can be observed that the peak position of the C═C stretching shifts from 1591 to 1582 cm^{-1} on changing from PPy to Au/PPy films. This may suggest that the Au/PPy film has better conductivity than the PPy film, which is in agreement with the conclusion based on the intensity difference between the two films described above. The peaks located at 1051.7 and 1055.8 cm^{-1} for PPy and Au/PPy films are assigned to the C−H in-plane deformation of oxidized PPy.[34]

Enhancement of the Raman signal intensity is larger as the Au deposition time increases or, likewise, the amount of deposited Au (data not shown) increases. The SERS effect observed for the Au/PPy films represents a convenient tool for qualitative analysis regarding the penetration of the gold electrodeposited inside the PPy matrix. Thus, by recording confocal Raman spectra at different depths in the PPy films, a gradual decrease in the intensity of the bands is observed, as expected for a resultant decrease in the amount of GNPs inside the PPy matrix (Figure 12). Accordingly, electrodeposition of gold takes place not only on the outermost part of the PPy film in contact with the electrolyte solutions, but also along the inner channels of the complex PPy film structure. This indicates a good distribution of Au centers inside the porous structure and a large effective surface area of the electrocatalytic material. These features of the modified electrode seem suitable for its use in an electrochemical sensor or for the electro-oxidation or electroreduction of species of interest in the field of electrocatalysis.

3.5. Electrocatalytic Properties of Au Decorated PPy/SS Electrodes. Electro-oxidation of Hydrazine and Hydroxylamine. In order to evaluate the electrocatalytic properties of the Au-decorated PPy/SS composite electrodes, voltammetric oxidations of hydrazine and hydroxylamine were studied. Voltammograms recorded on the PPy/SS electrodes do not contain anodic current contributions in the potential window for the electro-oxidation of these species. It should also be noted that the sensitive detection of these molecules is of particular interest in the field of environmental and biological analysis.[12,17,38] The overall oxidation reaction for hydrazine can be expressed as

$$N_2H_5^+ \rightarrow N_2(g) + 5H^+ + 4e^- \quad (1)$$

and for hydroxylamine

$$2NH_2OH + 4OH^- \rightarrow N_2O(g) + 5H_2O + 4e^- \quad (2)$$

Accordingly, these reactions are pH-dependent and it has been shown that the electro-oxidation current of both processes reach a maximum at pH 7.[12] Therefore, we performed the voltammetric electro-oxidation of both $N_2H_5HSO_4$ and NH_2OH in a phosphate buffer solution (PBS) with pH 7.

Positive-going potential scans run between −0.4 and 0.6 V with Au/PPy/SS electrodes in 0.1 M PBS containing 1×10^{-3} M hydroxylamine exhibit a rather broad anodic current peak that increases and shifts toward more positive potentials as the scan rate is increased (Figure 13a). The peak current exhibits a linear relationship when plotted against the square root of scan

DOI: 10.1021/am507733b
ACS Appl. Mater. Interfaces 2015, 7, 2677−2687

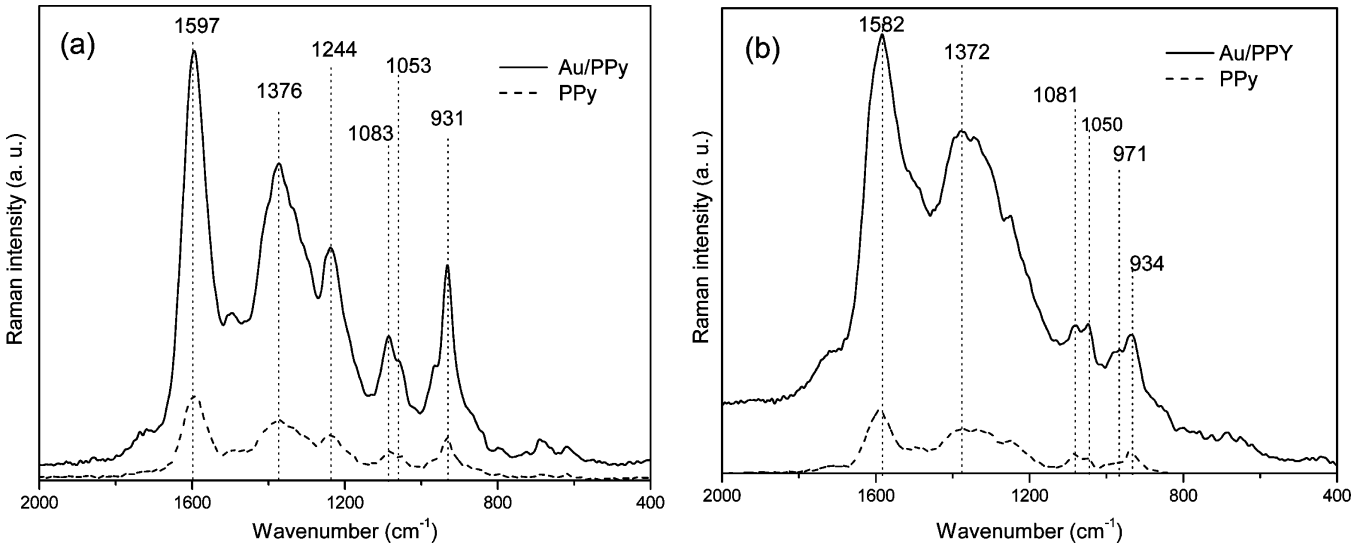

Figure 11. Raman spectra of PPy and PPy/Au films formed on a SS electrode. The PPy film was formed at 0.8 V during 10 min in 0.1 M $KClO_4$ (a) and in 0.5 M $C_7H_5NaO_3$ (b). Nucleation and growth time for Au electrodeposition were 0.1 and 5 s, respectively.

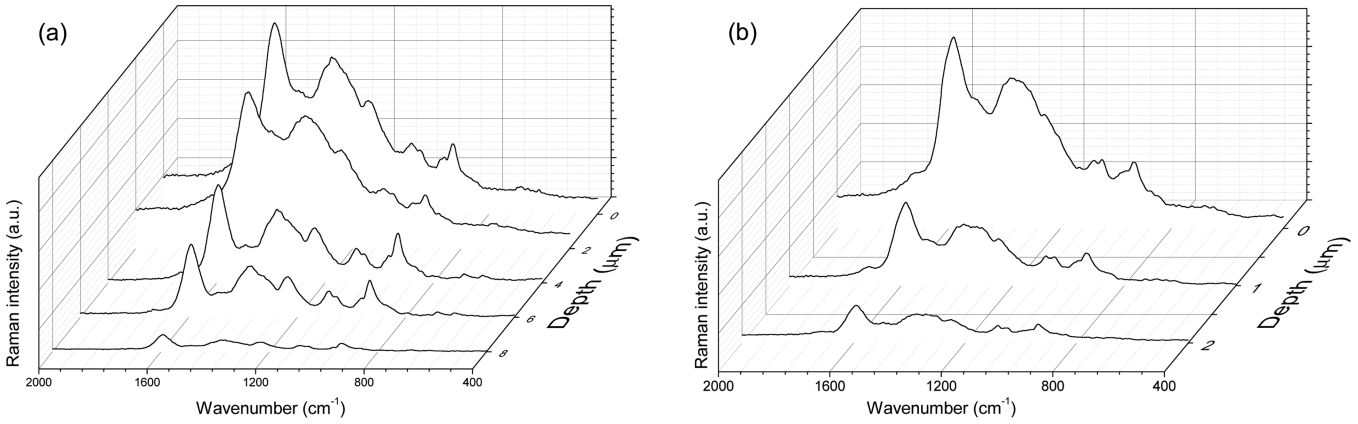

Figure 12. Confocal Raman spectra obtained at different depth inside Au-decorated PPy films. PPy films formed at 0.8 V during 10 min in 0.1 M $KClO_4$ (a) and 0.5 M $C_7H_5NaO_3$ (b). Nucleation and growth times for Au electrodeposition were 0.1 and 5 s, respectively.

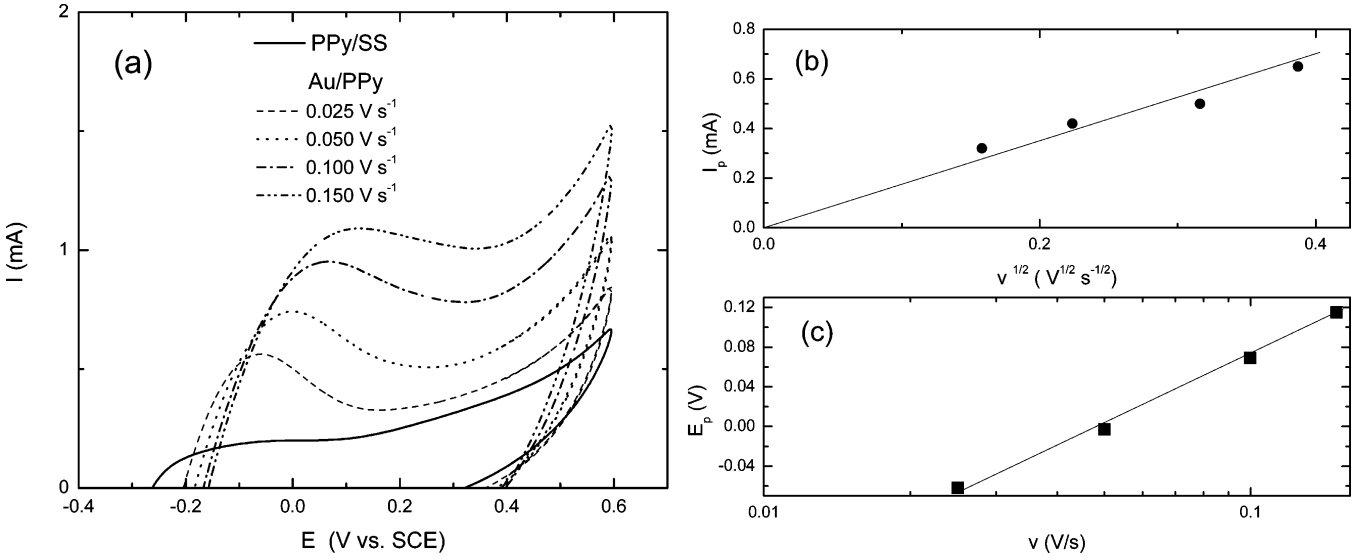

Figure 13. (a) Voltammograms of hydroxylamine electro-oxidation on Au/PPy/SS mesh electrode run at different scan rates. (b) Peak current and (c) peak potential dependencies on the scan rate. PPy film was grown for 5 min, nucleation and growth times for Au electrodeposition were 0.1 and 5 s, respectively. For the sake of simplicity only the positive-going scans are shown.

DOI: 10.1021/am507733b
ACS Appl. Mater. Interfaces 2015, 7, 2677−2687

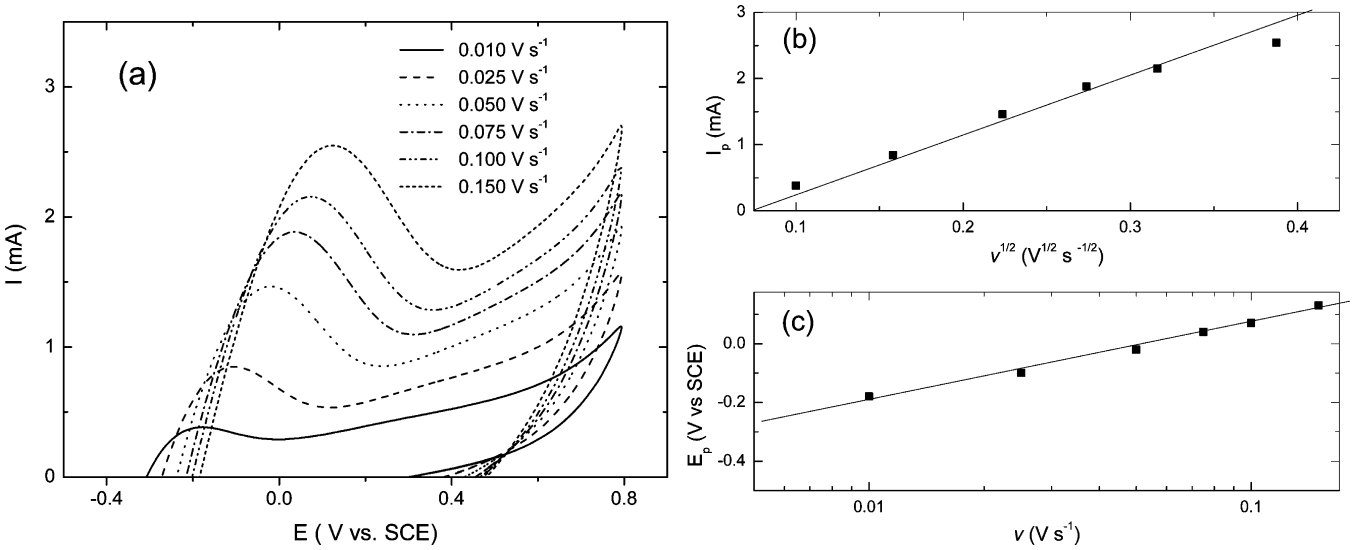

Figure 14. (a) Voltammograms of hydrazine electro-oxidation on Au/PPy/SS mesh electrode run at different scan rates. (b) Peak current and (c) peak potential dependencies on the scan rate. PPy film grown for 5 min; nucleation and growth times for Au electrodeposition were 0.1 and 5 s, respectively. For the sake of simplicity only the positive-going scans are shown.

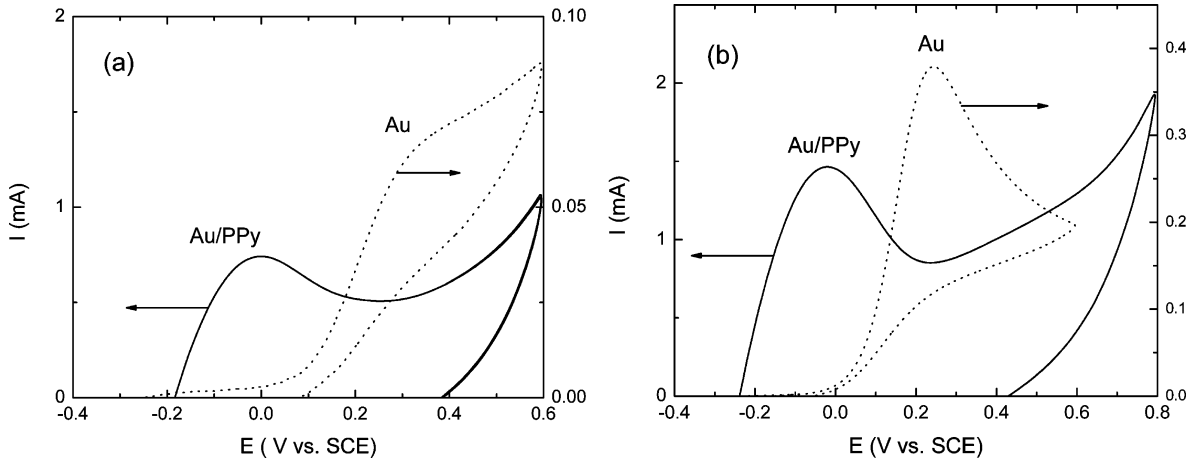

Figure 15. Voltammograms recorded on Au/PPy/SS mesh and Au bare electrodes in 0.1 M PBS (pH 7.0) containing 1×10^{-3} M $(NH_3OH)Cl$ (a) and 1×10^{-3} M $N_2H_4SO_4$ (b). $\nu = 0.05$ V s^{-1}. $t_{PPy} = 5$ min, $t_n = 0.1$ s, $t_c = 30$ s.

rate ν in the range of 0.010−0.4 V s^{-1} (Figure 13b). On the other hand, the peak potential is linearly dependent on log ν (Figure 13c), as expected for an irreversible electrochemical reaction under diffusion control.[39]

Similar results are obtained in the case of hydrazine. Voltammograms run at different scan rates also show the appearance of an anodic current peak when the PPy matrix is decorated with gold atoms (Figure 14a), and again according to an irreversible reaction under diffusion control, the current peak increases linearly with the square root of ν and the peak potential increases linearly with log ν (Figure 14b,c).

These results show that the composite electrodes are active for the electro-oxidation of both compounds. Figure 15 shows comparative voltammograms in the same solutions using the gold-decorated composite electrode in the form of a mesh and a bare smooth gold electrode. The voltammetric experiments performed at 0.050 V s^{-1} show that the electro-oxidation of both molecules occur on Au/PPy/SS electrodes at much lower anodic overpotentials than on bare gold (Figure 15). In the case of hydrazine, the electro-oxidation current peak appears approximately 0.25 V less positive than on bare gold, whereas for hydroxylamine, the difference is seemingly larger (ca. 0.35 V). Such an increase in the electrocatalytic activity of the composite electrodes, as compared to a smooth gold electrode, indicates that the gold decoration of the PPy matrix film deposited on a SS substrate generates not only a large area electrode, but also a good sensor for detecting analytes that are electrochemically active on gold.

4. CONCLUSIONS

A new effective strategy was implemented to assess the impact of alternative synthetic routes on the resulting electrode properties comparatively, namely, the type of substrate, the type of doping anion used during pyrrole electropolymerization, the electrodeposition program for the GNPs that involves optimization of the electrical variables, and so forth. This represents a distinct and necessary improvement on previous work in the field of metal nanoparticles/conducting polymer nanocomposites for electrochemical sensors. From the materials characterization point of view a particularly innovative approach has been presented in this work regarding the use of

DOI: 10.1021/am507733b
ACS Appl. Mater. Interfaces 2015, 7, 2677−2687

confocal Raman microscopy. These results represent not only a depth-profiling of the polymer film in the presence of GNPs, but the presence of electrodeposited particles clearly makes evident that these locations within the polymer matrix will be able to act as electroactive sites when the material is used in electrochemical sensing operations. The structure of the PPy matrix on SS substrates resulted in more compact, worm-like forms when prepared in 0.1 M $KClO_4$ solution, whereas an opened columnar structure was produced in 0.5 M $C_7H_5NaO_3$. The double potential-step routine allowed a fine control of the amount and size of GNPs deposited on PPy, in the form of a well-dispersed nanoarray even at positions deep inside the PPy matrix. The enhanced electrocatalytic behavior of these electrodes, as compared to flat Au surfaces, was successfully tested for the electro-oxidation of hydrazine and hydroxylamine, two molecules of particular interest in the field of electrochemical sensing.

AUTHOR INFORMATION

Corresponding Authors

*E-mail: aebolzan@inifta.unlp.edu.ar.
*E-mail: gervasi@inifta.unlp.edu.ar.

Notes

The authors declare no competing financial interest.

ACKNOWLEDGMENTS

This work was financially supported by the Agencia Nacional de Promoción Cientfica y Tecnológica of Argentina (ANPCYT, PICT 2013-0387), the Consejo Nacional de Investigaciones Científicas y Técnicas (CONICET) and the Comisión de Investigaciones Científicas de la Provincia de Buenos Aires (CICPBA). A.E.B. and C.A.G. are members of CICPBA.

REFERENCES

(1) Ansari Khalkhali, R. Electrochemical Synthesis and Characterization of Electroactive Conducting Polypyrrole Polymers. *Russ. J. Electrochem.* **2005**, *41*, 950−955.

(2) Li, J.; Lin, X.-Q. Electrodeposition of Gold Nanoclusters on Overoxidized Polypyrrole Film Modified Glassy Carbon Electrode and its Application for the Simultaneous Determination of Epinephrine and Uric Acid Under Coexistence of Ascorbic Acid. *Anal. Chim. Acta* **2007**, *596*, 222−30.

(3) Nowicka, A. M.; Fau, M.; Rapecki, T.; Donten, M. Polypyrrole-Au Nanoparticles Composite as Suitable Platform for DNA Biosensor with Electrochemical Impedance Spectroscopy Detection. *Electrochim. Acta* **2014**, *140*, 65−71.

(4) González, M.; Saidman, S. Electrodeposition of Polypyrrole on 316L Stainless Steel for Corrosion Prevention. *Corros. Sci.* **2011**, *53*, 276−282.

(5) Ma, R.; Sask, K.; Shi, C.; Brash, J.; Zhitomirsky, I. Electrodeposition of Polypyrrole-Heparin and Polypyrrole-Hydroxyapatite Films. *Mater. Lett.* **2011**, *65*, 681684.

(6) Gopi, D.; Indira, J.; Kavitha, L. Corrosion Protection Performance of Porous Strontium Hydroxyapatite Coating on Polypyrrole Coated 316L Stainless Steel. *Colloids Surf., B* **2013**, *107*, 130−136.

(7) Wang, J.; Chen, J.; Wang, C.; Zhou, D.; Too, C.; Wallace, G. Electrochemical Synthesis of Polypyrrole Films using Stainless Steel Mesh as Substrate for Battery Application. *Synth. Met.* **2005**, *153*, 117−120.

(8) Song, H.-K.; Palmore, G. Redox-Active Polypyrrole: Toward Polymer-Based Batteries. *Adv. Mater.* **2006**, *18*, 1764−1768.

(9) Li, X.; Zhitomirsky, I. Electrodeposition of PolypyrroleCarbon Nanotube Composites for Electrochemical Supercapacitors. *J. Power Sources* **2013**, *221*, 49−56.

(10) Si, P.; Ding, S.; Lou, X.-W. D.; Kim, D.-H. An Electrochemically formed Three-Dimensional Structure of Polypyrrole/Graphene Nanoplatelets for High-Performance Supercapacitors. *RSC Adv.* **2011**, *1*, 1271.

(11) Oukil, D.; Benhaddad, L.; Makhloufi, L.; Aitout, R.; Saidani, B. Gold Nanoparticles Modified Polypyrrole/Iron Electrode Used as Sensor for Hydrazine Detection. *Sens. Lett.* **2013**, *11*, 395−404.

(12) Li, J.; Lin, X. Electrocatalytic Oxidation of Hydrazine and Hydroxylamine at Gold NanoparticlePolypyrrole Nanowire Modified Glassy Carbon Electrode. *Sens. Actuators, B* **2007**, *126*, 527−535.

(13) González, M. B.; Quinzani, O. V.; Vela, M. E.; Rubert, A. A.; Benítez, G.; Saidman, S. B. Study of The Electrosynthesis of Hollow Rectangular Microtubes of Polypyrrole. *Synth. Met.* **2012**, *162*, 1133−1139.

(14) An, T.; Choi, W.; Lee, E.; Cho, S. J.; Lim, G. Fabrication of Conducting Polymer Micro/Nanostructures Coated with Au Nanoparticles for Electrochemical Sensors. *J. Nanosci. Nanotechnol.* **2012**, *12*, 4975−4978.

(15) Singh, S.; Jain, D. V. S.; Singla, M. L. One Step Electrochemical Synthesis of Gold-Nanoparticles Polypyrrole Composite for Application in Catechin Electrochemical Biosensor. *Anal. Methods* **2013**, *5*, 1024.

(16) Maduraiveeran, G.; Ramaraj, R. A Facile Electrochemical Sensor Designed from Gold Nanoparticles Embedded in Three-Dimensional SolGel Network for Concurrent Detection of Toxic Chemicals. *Electrochem. Commun.* **2007**, *9*, 2051−2055.

(17) Li, J.; Xie, H.; Chen, L. A Sensitive Hydrazine Electrochemical Sensor Based on Electrodeposition of Gold Nanoparticles on Choline Film Modified Glassy Carbon Electrode. *Sens. Actuators, B* **2011**, *153*, 239−245.

(18) Chen, W.; Li, C. M.; Chen, P.; Sun, C. Electrosynthesis and Characterization of Polypyrrole/Au Nanocomposite. *Electrochim. Acta* **2007**, *52*, 2845−2849.

(19) Abdul Aziz, M.; Kawde, A.-N. Gold Nanoparticle-Modified Graphite Pencil Electrode for the High-Sensitivity Detection of Hydrazine. *Talanta* **2013**, *115*, 214−21.

(20) Li, X.; Zhitomirsky, I. Capacitive Behaviour of Polypyrrole Films Prepared on Stainless Steel Substrates by Electropolymerization. *Mater. Lett.* **2012**, *76*, 15−17.

(21) Hallik, A.; Alumaa, A.; Tamm, J.; Sammelselg, V.; Väärtnõu, M.; Jänes, A.; Lust, E. Analysis of Electrochemical Impedance of Polypyrrole—Sulfate and Polypyrrole—Perchlorate Films. *Synth. Met.* **2006**, *156*, 488−494.

(22) Li, J.; Xie, H.; Li, Y. Fabrication of Gold Nanoparticles/Polypyrrole Composite-Modified Electrode for Sensitive Hydroxylamine Sensor Design. *J. Solid State Electrochem.* **2011**, *16*, 795−802.

(23) Wang, L.; Bai, J.; Huang, P.; Wang, H.; Zhang, L.; Zhao, Y. Self-Assembly of Gold Nanoparticles for the Voltammetric Sensing of Epinephrine. *Electrochem. Commun.* **2006**, *8*, 1035−1040.

(24) Hermas, A.; Nakayama, M.; Ogura, K. Formation of Stable Passive Film on Stainless Steel by Electrochemical Deposition of Polypyrrole. *Electrochim. Acta* **2005**, *50*, 3640−3647.

(25) Gopi, D.; Govindaraju, K.; Kavitha, L.; Basha, K. A. Synthesis, Characterization and Corrosion Protection Properties of Poly(N-Vinyl Carbazole-Co-Glycidyl Methacrylate) Coatings on Low Nickel Stainless Steel. *Prog. Org. Coat.* **2011**, *71*, 11−18.

(26) Gopi, D.; Saraswathy, R.; Athithya, G.; Kavitha, L.; Bae, J.-H.; Kim, D.-K. Corrosion Protection Performance of Ceria-Copolymer Bilayer Coating on Low Nickel Stainless Steel in 0.5 M H_2SO_4 Medium. *Surf. Interface Anal.* **2012**, *44*, 1331−1337.

(27) Gopi, D.; Indira, J.; Kavitha, L. Hydroxyapatite Coating on Selectively Passivated and Sensitively Polymer Protected Surgical Grade Stainless Steel. *J. Appl. Electrochem.* **2013**, *43*, 331−345.

(28) Ramaraj, R.; Maduraiveeran, G. In *Nanostructured Materials for Electrochemical Biosensors*; Yogeswaran, U., Kumar, S., Chen, S., Eds.; Nova Science Publishers, Inc.: New York, 2009; Chapter 3, pp 65−95.

(29) Cascalheira, A.; Aeiyach, S.; Lacaze, P.; Abrantes, L. Electrochemical Synthesis and Redox Behaviour of Polypyrrole Coatings on

DOI: 10.1021/am507733b
ACS Appl. Mater. Interfaces 2015, 7, 2677−2687

Copper in Salicylate Aqueous Solution. *Electrochim. Acta* **2003**, *48*, 2523−2529.
(30) Láng, G.; Ujvári, M.; Rokob, T.; Inzelt, G. The Brush Model of the Polymer Films−Analysis of the Impedance Spectra of Au,Pt—Poly(O-Phenylenediamine) Electrodes. *Electrochim. Acta* **2006**, *51*, 1680−1694.
(31) Liu, Y.-C. Characteristics of Vibration Modes of Polypyrrole on Surface-Enhanced Raman Scattering Spectra. *J. Electroanal. Chem.* **2004**, *571*, 255−264.
(32) Lyons, M. In *Electroactive Polymer Electrochemistry*; Lyons, M., Ed.; Plenum Press: New York, 1994; Vol. *1*.
(33) Nguyen Thi Le, H. Raman Spectroscopy Analysis of Polypyrrole Films as Protective Coatings on Iron. *Synth. Met.* **2004**, *140*, 287−293.
(34) Liu, Y.-C.; Hwang, B.-J. Identification of Oxidized Polypyrrole on Raman Spectrum. *Synth. Met.* **2000**, *113*, 203−207.
(35) Dietz, H.; Sandmann, G.; Anders, A.; Plieth, W. In *Raman Spectroscopy for Nanomaterials Characterization*; Kumar, C., Ed.; Springer: Berlin, 2012; pp 167−190.
(36) Palys, B.; Bukowska, J.; Jackowska, K. SERS of 1,8-Diaminonaphthalene on Gold, Silver and Copper Electrodes Polymerisation and Complexes Formed with the Electrode Material. *J. Electroanal. Chem.* **1997**, *428*, 19−24.
(37) Kim, D.; Lee, J.; Moon, D.; Kim, C. Stability of Reduced Polypyrrole. *Synth. Met.* **1995**, *69*, 471−474.
(38) Tang, Y.-Y.; Kao, C.-L.; Chen, P.-Y. Electrochemical Detection of Hydrazine Using a Highly Sensitive Nanoporous Gold Electrode. *Anal. Chim. Acta* **2012**, *711*, 32−9.
(39) Bard, A. J.; Faulkner, L. R. *Electrochemical Methods. Fundamentals and Applications*, 2nd ed.; John Wiley & Sons: New York, 2001.

DOI: 10.1021/am507733b
ACS Appl. Mater. Interfaces 2015, 7, 2677−2687